Resonant Raman-active localized vibrational modes in $Al_yGa_{1-y}N_xAs_{1-x}$ alloys: Experiment and first-principles calculations

A. M. Teweldeberhan,[1] G. Stenuit,[1] S. Fahy,[1,2] E. Gallardo,[3] S. Lazić,[3] J. M. Calleja,[3] J. Miguel-Sánchez,[4] M. Montes,[4] A. Hierro,[4] R. Gargallo-Caballero,[4] A. Guzmán,[4] and E. Muñoz[4]

[1]*Tyndall National Institute, Lee Maltings, Prospect Row, Cork, Ireland*

[2]*Department of Physics, University College Cork, Cork, Ireland*

[3]*Departamento de Física de Materiales, Universidad Autónoma de Madrid, E-28049 Madrid, Spain*

[4]*Instituto de Sistemas Optoelectrónicos y Microtecnología, Universidad Politécnica de Madrid, E-28040 Madrid, Spain*

(Received 17 December 2007; revised manuscript received 24 February 2008; published 16 April 2008)

The localized vibrational modes associated with substitutional aluminium and nitrogen atoms in $Al_yGa_{1-y}N_xAs_{1-x}$ have been studied within first-principles density functional theory using a supercell approach. Localized vibrational modes related to N-Al_mGa_{4-m} ($1 \leqslant m \leqslant 4$) complexes have been identified, which reveal the formation of N-Al_4 units well above random abundance, in qualitative agreement with a large calculated value (391 meV) of the Al-N bond formation energy. We determine the resonant Raman-active modes from the selection rule obtained by calculating the electron-phonon coupling strength and optical transition matrix elements and compare them with resonant Raman spectroscopy measurements. The localized modes from Raman scattering measurements with frequencies around 325, 385, 400, 450, 500, and 540 cm^{-1} are found to be in good agreement with the calculated modes (326, 364, 384, 410, 456, 507, and 556 cm^{-1}). The modes are classified as follows: the two modes at 326 and 556 cm^{-1} belong to the N-$AlGa_3$ configuration; there are three modes which belong to N-Al_2Ga_2 with frequencies at 326, 364, and 507 cm^{-1}; the N-Al_3Ga configuration gives rise to modes whose frequencies are 384 and 456 cm^{-1}; and the mode at a frequency of 410 cm^{-1} belongs to the N-Al_4 complex. The comparison of line intensities from samples before and after rapid thermal annealing allows us to experimentally distinguish vibrational modes associated with different clusters, in agreement with the theoretical assignments.

DOI: 10.1103/PhysRevB.77.155208 PACS number(s): 71.15.−m, 63.20.Pw, 78.20.Ek, 71.55.Eq

I. INTRODUCTION

The ternary (GaNAs) and quaternary (InGaNAs and AlGaNAs) dilute nitride alloys have attracted considerable interest in recent years both because of their fundamental physical properties and potential device applications. When a small fraction of As atoms in these alloys are replaced by N, the energy gap decreases rapidly; for example, by 150 meV when 1% of N is added to GaAs.[1] This makes the nitride alloys promising candidates for long wavelength (1.3 and 1.5 μm) telecommunication lasers based on GaAs substrates[2] and for extending the wavelength range of GaAs-based solar cells further into the infrared.[3]

Because of the small masses of nitrogen and aluminium and the strength of Ga-N and Al-N bonds, localized vibrational modes which are specifically related to the simultaneous presence of N and Al exist in AlGaNAs. Localized vibrational mode (LVM) spectroscopy is a useful technique for studying the local bonding of impurities and impurity complexes in semiconductors.[4–6] Substantial experimental work,[7–18] using both Raman and infrared spectroscopies, has been done to study the LVM caused by the incorporation of N into GaAs, InGaAs, and AlGaAs. The pressure dependence of the frequency of the LVM of substitutional nitrogen in the dilute nitride, GaN_xAs_{1-x}, has been recently studied in Ref. 19 within first-principles density functional theory (DFT) using a supercell approach. The same technique has been used to study the effect of the substitution of nearest-neighbor gallium atoms by indium[20] on the frequency of the LVM. In this paper, we study the localized modes associated with substitutional Al and N atoms in AlGaNAs using first-principles density functional theory. We also calculate the electron-phonon coupling strength and optical transition matrix elements to determine the resonant Raman-active LVMs and compare them with experimental data.

The rest of the paper is organized as follows. The computational details are described in Sec. II. The experimental procedure is presented in Sec. III. In Sec. IV, we present and discuss the theoretical and experimental results. A summary is given in Sec. V.

II. COMPUTATIONAL DETAILS

First-principles, pseudopotential, plane-wave, density functional theory methods allow us to calculate electronic ground state energies and atomic forces for a given arrangement of atoms in a periodic structure, without fitting to experimental data. Although systems treated in this approach are always formally periodic in three dimensions, supercell methods are used to treat surface or defect structures, such as substitutional nitrogen in GaAs.[19,21] Within this approach, reliable results are obtained from large supercells because interactions between impurities in the neighboring supercells are weak. However, calculation of the full dynamical matrix (DM) is computationally very demanding for large supercells. Therefore, it is important to choose the smallest possible supercell size that produces reliable results for the problem under investigation.

A 32-atom body-centered cubic supercell is used in these calculations. Finite-size convergence tests were performed

 ©2008 The American Physical Society

with a larger supercell (64 atoms) by fixing all atoms in the supercell except the nitrogen and aluminium atoms to verify that the mode frequencies are well converged[34] in the 32-atom cell.[19,20] In each case, a nitrogen atom is substituted on one arsenic site and m ($m \leqslant 4$) aluminium atoms are substituted on nearest-neighbor gallium sites of the GaAs lattice. The positions of all atoms within the supercell and the supercell dimensions are then relaxed to minimize the ground state energy of the system. Once the fully relaxed structure is obtained, we use the finite dynamical matrix approach, whereby harmonic restoring forces are found by small displacements of each atom from its equilibrium position, calculating the resulting forces on all atoms using the Hellmann–Feynman (HF) theorem.[22]

We find the ground state electronic energy and the HF forces in density functional theory using the VASP code,[23,24] which solves the Kohn–Sham equations by an iterative diagonalization scheme in a plane-wave basis set. The local density approximation (LDA) for the exchange-correlation functional is used, as parametrized by Perdew and Zunger.[25] The calculations have been performed using ultrasoft pseudopotentials[26,27] and the $3d$ states are included as valence states for Ga atoms. The plane-wave cutoff energy was set at 452 and 348 eV for structural relaxation and calculation of the forces, respectively. The method of special $\vec{k}$-point generation based on the Monkhorst–Pack[28] scheme is used for $\vec{k}$-point sampling. We have used a $4\times4\times4$ mesh for the 32-atom supercell and a $2\times2\times2$ mesh for the 64-atom supercell. The structures were optimized until the residual HF forces were less than or equal to 10^{-4} eV/Å.

A. Calculation of localized vibrational modes

The vibrational mode frequencies and amplitudes of vibration are determined by direct diagonalization of the full DM, which is obtained from the force constant matrix. Within the harmonic approximation, the total energy of a supercell with small displacements of atoms from their equilibrium positions is given by

$$E = E_0 + \frac{1}{2}\sum_{i,j,\alpha,\beta} \Phi_{\alpha\beta}(i,j) d_\alpha(i) d_\beta(j), \tag{1}$$

where $d_\alpha(i)$ is the displacement of atom i from its equilibrium position in the direction α. The small displacement $d_\beta(j)$ of atom j in the direction β induces a force on atom i in the direction α as

$$F_\alpha(i) = -\Phi_{\alpha\beta}(i,j) d_\beta(j). \tag{2}$$

Once the optimized structure is obtained, we compute the real-space force constant matrix $\Phi_{\alpha\beta}(i,j)$ by calculating the HF forces $F_\alpha(i)$ induced by making displacements d_0 [$d_\beta(j)=d_0=0.01a$, where a is the lattice constant] of each atom j in the supercell in three orthogonal directions, $\beta=1,2,3$. We have considered both $+d_0$ and $-d_0$ and a central difference of the corresponding forces is used to calculate the force constant matrix. The DM, $D_{\alpha\beta}(i,j) = (M_i M_j)^{-1/2}\Phi_{\alpha\beta}(i,j)$, is then constructed (where M_i is the mass of atom i) and diagonalized to obtain the eigenvalues, $e_k=\omega_k^2$, and the normalized eigenvectors, $|u_k\rangle$, where $\langle i,\alpha|u_k\rangle = u_k(i,\alpha) = \sqrt{M_i}s_k(i,\alpha)$ and $s_k(i,\alpha)$ is the amplitude of motion of atom i in the α direction for vibrational mode k. Modes with frequencies outside the range of the GaAs phonon bands (i.e., with frequency greater than 287 cm^{-1}) are considered to be localized. These modes are also found to have a large amplitude of motion on the light (N and Al) atoms.

B. Selection rule for resonant Raman scattering

The interactions between lattice vibrations and electronic states can be studied through the resonant Raman scattering (RRS). The Raman scattering probability for the Stokes scattering process can be written in a simplified form as[29,30]

$$I_{ph}(\omega_s) = \left(\frac{2\pi}{\hbar}\right)\left|\sum_{n,n'} \frac{\langle i|H_{eR}|n'\rangle\langle n'|H_{e\text{-}ph}|n\rangle\langle n|H_{eR}|i\rangle}{[\hbar\omega_i - (E_n - E_i)][\hbar\omega_i - \hbar\Omega - (E_{n'} - E_i)]}\right|^2 \delta(\hbar\omega_i - \hbar\Omega - \hbar\omega_s), \tag{3}$$

where H_{eR} and $H_{e\text{-}ph}$ are the electron-radiation and electron-phonon interaction Hamiltonians, $|i\rangle$ is the initial electronic state, $|n\rangle$ is the intermediate electronic state with energy E_n, $\hbar\omega_i$ and $\hbar\omega_s$ are the energies of the incident and scattered photons, respectively, and $\hbar\Omega$ is the energy of the phonon being studied, i.e., associated with the LVMs in the material. For electron scattering near resonance with an intermediate state $|n\rangle$, we use an adiabatic approximation assuming that the emitted phonon related to the displacement of atoms in localized mode does not significantly modify the other intermediate state $|n'\rangle$, i.e., $|n'\rangle=|n\rangle$. Under this assumption, the RRS selection rule can be obtained by combining the three contributions in the numerator of Eq. (3), i.e., (1) a Bloch state $|n\rangle$ with energy E_n at the Γ point excited by a photon with energy $\hbar\omega_i=E_n-E_i$, (2) the electron-phonon coupling between the state $|n\rangle$ and the LVM, and (3) the reemission of a photon with energy $\hbar\omega'=\hbar\omega_i-\hbar\Omega$. Thus, the RRS intensity becomes proportional to

$$I_{ph}(\omega_s) \propto |\langle i|H_{eR}|n\rangle\langle n|H_{e\text{-}ph}|n\rangle\langle n|H_{eR}|i\rangle|^2. \tag{4}$$

The electron-radiation coupling term in Eq. (4) may be estimated by the dipole approximation, where only zone-centered phonons with momentum $\mathbf{q}=0$ are involved in the light scattering process. The expectation value $\langle n|H_{eR}|i\rangle$ is

then given by the dipole transition matrix elements,

$$|\langle n|H_{eR}|i\rangle|^2 \propto P_n = |\langle n|\hat{p}|i\rangle|^2 = \left|\sum_{\mathbf{G}} \mathbf{G} C_n^*(\mathbf{G}) C_i(\mathbf{G})\right|^2, \quad (5)$$

where the sum runs over the vectors of the reciprocal space and $C_n(\mathbf{G})$ and $C_i(\mathbf{G})$ are the coefficients of the plane-wave expansion of the electronic Bloch states $|n\rangle$ and $|i\rangle$ at the Γ point, respectively. Since we are interested in RRS produced by incident photons with energies of the order of the energy gap ($\hbar\omega_i \approx 1-2$ eV), the optical transitions involved in the RRS will occur from the valence band maximum ($|i\rangle$) to an excited state in the conduction band ($|n\rangle$). The energy E_n of the intermediate state $|n\rangle$ is then defined relative to the valence band maximum (VBM).

The middle matrix elements in Eq. (4) (the electron-phonon coupling) can be evaluated from the classical relation,[31]

$$\langle n|H_{e\text{-}ph}|n\rangle \propto g(n,n,\Omega) = \left(\frac{\hbar}{2M\Omega}\right)^{1/2} \langle n|\hat{\epsilon}_\Omega \cdot \vec{\nabla} V_{sc}|n\rangle = \left(\frac{\hbar}{2M\Omega}\right)^{1/2} \hat{\epsilon}_\Omega \cdot \frac{\partial E_n}{\partial \mathbf{Q}}, \quad (6)$$

where $\hat{\epsilon}_\Omega$ is the phonon polarization vector and $\vec{\nabla} V_{sc}$ is the gradient of the self-consistent potential with respect to the phonon coordinate $\mathbf{Q}$. Equation (6) has been obtained using the HF theorem.[22]

From Eqs. (4)–(6), one can estimate the selection rule for the RSS using

$$I_{ph} \propto \left| P_n \frac{\partial E_n}{\partial \mathbf{Q}} \right|^2. \quad (7)$$

The above relation can also be obtained from the semiclassical approach, where the Raman scattering cross section is proportional to $|\partial\chi/\partial\mathbf{Q}|^2$, the square of the derivative of the optical polarizability χ with respect to the phonon coordinate $\mathbf{Q}$. In this case, the optical polarizability is proportional to

$$\chi(\omega) \propto \sum_n \frac{P_n}{\omega - E_n/\hbar}, \quad (8)$$

where n labels the optical transitions and E_n is the transition energy (the difference between the final and initial energies). Differentiation of Eq. (8) gives

$$\frac{\partial\chi}{\partial\mathbf{Q}} \propto \sum_n \frac{P_n}{(\omega - E_n/\hbar)^2} \frac{\partial E_n}{\partial \mathbf{Q}}. \quad (9)$$

From Eq. (9), one can clearly see that the derivative of the optical transition energy E_n with respect to the phonon coordinate $\mathbf{Q}$ and the optical transition matrix elements near resonance ($\hbar\omega \approx E_n$) give the RRS.

The dipole transition matrix elements and the shift of the electronic level E_n with respect to the amplitudes of motion of the atoms for each LVM have been computed from our DFT calculations performed with the 32-atom cell.

III. EXPERIMENT

The samples studied are 500 nm thick layers of $Al_{0.22}Ga_{0.78}N_xAs_{1-x}$ grown on GaAs substrates by molecular beam epitaxy using a radio-frequency plasma source for the supply of atomic nitrogen. The layers were capped with a 100 nm GaAs layer. Different N concentrations up to $x = 0.01$ were obtained by varying the substrate temperature. The N concentration was roughly estimated using x-ray diffraction from the shift of the diffraction peak with respect to that of AlGaAs in θ-2θ scans. Postgrowth rapid thermal annealing at 700–900 °C was carried out for 30 s in some of the samples to distinguish the LVMs associated with the different complexes. RRS spectra were recorded in backscattering geometry at room and low temperature using Ti-sapphire and dye lasers as excitation sources and a double-grating spectrometer with a charged coupled device detector. A continuous flow cryostat with He-exchange gas was used for low temperature (77 K) measurements.

IV. RESULTS

There are several localized modes associated with N and Al (i.e., with frequencies above the continuum phonon band edge) in this alloy. Here, we focus on the modes which are resonant Raman-active ($I_{ph} \neq 0$) in order to compare our theoretical results with the RRS measurements. The intensities of the resonant Raman-active modes estimated from the electron-phonon coupling strength and optical transition matrix elements as a function of the conduction band energies relative to the VBM are shown in Fig. 1(a). For incident photons with energy range of 0.2–1.6 eV, the frequencies of the resonant Raman-active LVMs originating from all possible configurations of nitrogen-centered clusters (N-Al_mGa_{4-m}, $1 \leqslant m \leqslant 4$) are calculated to be 326, 364, 384, 410, 456, 507, and 556 cm^{-1}. The modes are classified as follows: the two modes at 326 and 556 cm^{-1} belong to the N-$AlGa_3$ configuration; there are three modes which belong to N-Al_2Ga_2 with frequencies at 326, 364, and 507 cm^{-1}; the N-Al_3Ga configuration gives rise to modes whose frequencies are 384 and 456 cm^{-1}; and the mode at a frequency of 410 cm^{-1} belongs to the N-Al_4 complex.

The Raman spectra of two samples with 0.1% and 1% of N are shown in Fig. 1(b) for excitation energy of 1.96 eV. The extended GaAs-like (LO_1, TO_1) and AlAs-like (LO_2, TO_2) phonons of AlGaAs are observed, together with the LO mode of the GaAs substrate. In addition, six peaks at frequencies around 325, 385, 400, 450, 500, and 540 cm^{-1} [marked by arrows in Fig. 1(b)] are shown in the spectra. These peaks, some of which have been observed previously at room temperature,[11,13] are related to the simultaneous presence of Al and N. According to the DFT calculations, we can ascribe the new Raman peaks to LVMs of N-Al_mGa_{4-m} complexes of different m. The theoretical results for the Raman-active modes, represented by a different symbol for each cluster in Fig. 1(b), are in good agreement with the experimental data. The discrepancy between the calculated and the experimental values of the LVM frequencies is below 3%. Previous DFT calculations of known vibrational mode frequencies in semiconductors give a typical accuracy of a

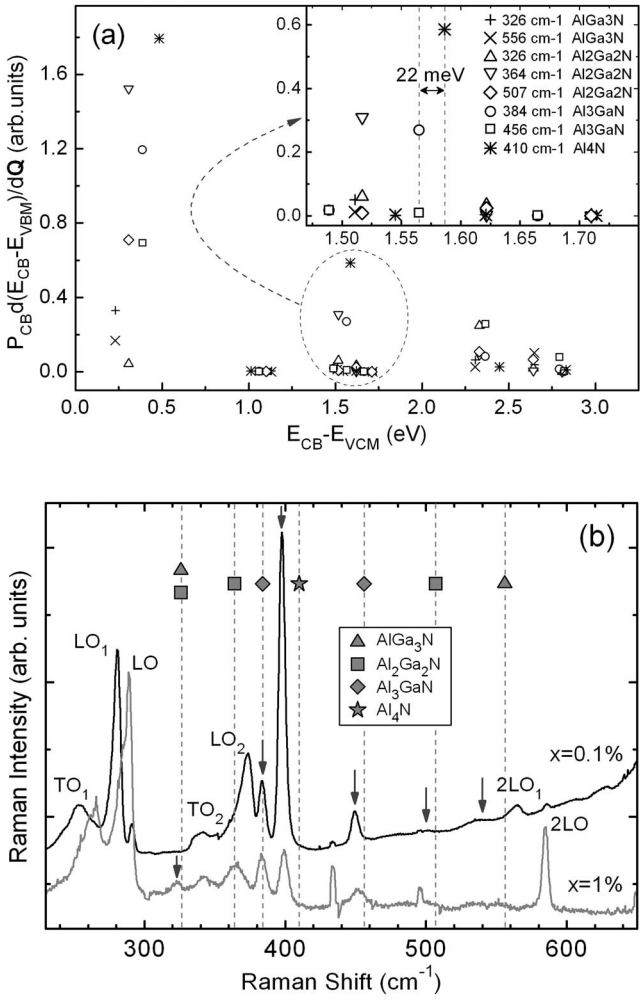

FIG. 1. (a) Estimated intensities $[P_{CB}\partial(E_{CB}-E_{VBM})/\partial\mathbf{Q}=|\langle CB|\hat{p}|VBM\rangle|^2\partial(E_{CB}-E_{VBM})/\partial\mathbf{Q}]$ as a function of the conduction band energies relative to the valence band maximum. The difference in resonance energies (22 meV) between the modes associated with N-Al_3Ga and N-Al_4 is shown in the inset. (b) Experimental Raman spectra at 77 K of dilute AlGaNAs films with 0.1% and 1% of N concentration. Experimental and theoretical LVMs are marked by arrows and symbols, respectively. Narrow peaks at 435 and 495 cm^{-1} are Ne spectral lines for calibration purposes.

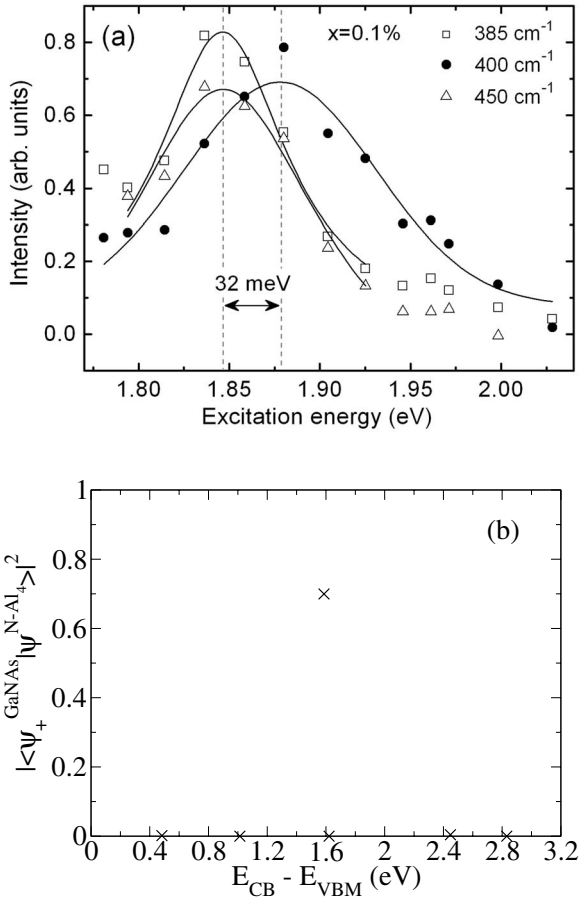

FIG. 2. (a) Experimental Raman resonance of the modes of complexes with $m=3$ and $m=4$ of the sample with 0.1% of N content. Solid lines are the Lorentz fits. (b) The projection of the wave function of the E_+ state in GaNAs onto the wave functions of conduction band states for the N-Al_4 configuration.

few percent. For example, the LVM frequency associated with substitutional N in GaAs has been calculated as 465 cm^{-1}, compared to an experimental value of 472 cm^{-1}.[19] The calculated mode at 364 cm^{-1} is probably obscured experimentally due to the AlAs-like LO_2 phonons observed around 365 cm^{-1}.

The intensities of the modes with $m=3$ and $m=4$ (peaks at 385, 400, and 450 cm^{-1}) of the sample with 0.1% of N as a function of the excitation energy in the range from 1.6 to 2 eV are shown in Fig. 2(a). The maxima of the Raman resonance profiles are normalized for easier comparison. RRS profiles of the LVMs belonging to $m=1,2$ complexes could not be obtained as the scattering intensities are too weak. The resonance maxima are well above the band gap, which is 1.58 eV at 77 K for this sample. The modes at 385 and 450 cm^{-1} ($m=3$) resonate at the same energy, which is 32 meV below the resonance energy of the peak at 400 cm^{-1} ($m=4$). Similar theoretical results are shown in the inset of Fig. 1(a) with a difference of 22 meV between the resonance energies of the modes with $m=3$ and $m=4$. The same behavior is observed in the sample with 1% of N concentration (not shown here), but in that case, the Raman resonance energies of the three modes are shifted to lower energies. Therefore, we conclude that the electronic transitions responsible for the observed resonances are linked to the different N-Al_mGa_{4-m} clusters. The large width (150–200 meV) of the experimental RRS profiles is attributed to alloy fluctuations, producing different surroundings of the N-Al_mGa_{4-m} complexes inside the scattering volume. Actually, the PL emission of the sample containing 0.1% N (not shown) has a similar width. Additionally, the possible presence of incoming and outgoing resonances in the RRS profile could contribute to the resonance width. As both resonances should be separated by about 50 meV, they are not experimentally be resolved.

The high intensity of the modes at 385 and 400 cm^{-1} in the sample with lower N content is attributed to its strong resonant enhancement, as compared to the sample with higher N content. Indeed, the maximum of the resonant profile of the 0.1% sample [1.88 eV, Fig. 2(a)] is closer to the

excitation energy (1.96 eV) than that of the 1% sample (1.80 eV, not shown). These intense modes correspond to $m=3$ and $m=4$ complexes, and although we would expect them to be very scarce in a random ion distribution, they might form with noticeable abundance due to the strong Al-N binding energy. This is experimentally confirmed by the significant reduction of the apparent Al concentration (Al bonded only to As atoms) upon increasing the growth temperature, as a result of mobility of the atoms of Al and N which can form the energetically more favorable Al-N bonds.[18] The formation energies of N-Al, N-Al_2, N-Al_3, and N-Al_4 bonds obtained from the 64-atom supercell calculations are 391, 788, 1173, and 1535 meV, respectively. The Al-N binding energy is much larger than that of In-N (197 meV) in InGaNAs (Ref. 20) and suggests that N-$AlGa_3$ and N-Al_2Ga_2 clusters would be very rare, even though actual growth does not give thermal equilibrium abundances. N-Al_4 should be the predominant cluster at thermal equilibrium. This is consistent with the low intensity of Raman scattering at mode frequencies associated with N-$AlGa_3$ and N-Al_2Ga_2 clusters. Based on the theoretical, thermal equilibrium values for abundance of various clusters ($m=1-4$), we would expect a large proportion of N-Al_4 clusters under actual growth conditions.

The experimental resonance energies at which the modes related to N-Al_3Ga and N-Al_4 were observed are associated with electronic transitions specific to each complex, which derive from the E_+ state found in the dilute GaNAs nitrides. In order to determine the character of the calculated states, we extracted the ψ_+ state in GaNAs [the singlet state above the CBE with a high optical transition matrix elements (see Ref. 32 for further details)] and projected it onto the conduction band states obtained from the N-Al_4 configuration. Figure 2(b) shows the probability $|\langle\psi_+|\psi_i^{\text{N-Al}_4}\rangle|^2$ versus the energies $E_{CB}-E_{VMB}$ of the different $\psi_i^{\text{N-Al}_4}$ states. As a result, we obtain that the $\psi_3^{\text{N-Al}_4}$ state giving rise to an active RRS at around 1.6 eV in Fig. 1(a) has about 70% of ψ_+ character. Therefore, the higher resonance energy levels can be associated with the E_+ state in GaNAs.

The discrepancy between our calculated photon energy range of 0.2–1.6 eV and the experimental range of 1.6–2.0 eV can be explained by (1) the LDA underestimation of the energy gap, which is found to be of the order of 1.0 eV for GaAs (Ref. 35) and (2) the higher nitrogen concentration used in the calculations ($x=6.25\%$) compared to the experimental concentrations $x=0.1\%$ and $x=1\%$. Our first-principles calculations in dilute $GaAs_{1-x}N_x$ nitrides[32] show that the energy separation $\Delta E=E_+-E_{CBE}$ reduces to 0.4 and 0.19 eV at $x=1\%$ and 0.1%, respectively. This is in agreement with Ref. 33 ($\Delta E=0.2$ eV at $x=0.1\%$). Therefore, the experimental resonance energy of about 1.8 eV observed at $x=0.1\%$ is in good agreement with our theoretical prediction $E_+=E_g+\Delta E=1.58$ eV+0.19 eV=1.77 eV. We would expect a small shift in the E_+ energy due to the substitution of Ga by Al in the clusters considered here. The calculated shift in resonance energy (22 meV), in going from N-Al_3Ga to N-Al_4, is in reasonably good agreement with the value (32 meV) found experimentally.

Since the E_+ state in GaNAs is localized around the nitrogen atoms for lower N concentration, we expect the coupling $\partial E_+/\partial\mathbf{Q}$ to remain large for the phonon coordinate $\mathbf{Q}$ of the LVMs, whereas the coupling $\partial E_{CBE}/\partial\mathbf{Q}$ to the conduction band edge will be weakened as the N concentration decreases. Thus, the resonant transition to the E_+ state is particularly sensitive to the LVMs associated with N.

V. CONCLUSIONS

The LVMs associated with substitutional aluminium and nitrogen atoms in AlGaNAs have been studied within first-principles density functional theory supercell calculations and compared to resonant Raman measurements. We find a good agreement between the calculated frequencies and the experimental values. The intensity of the modes estimated from the electron-phonon coupling strength and optical transition matrix elements will be useful in classifying the modes which belong to N-Al_mGa_{4-m} clusters experimentally.

ACKNOWLEDGMENTS

This work is supported by Science Foundation Ireland and the research contracts of the Spanish Ministry of Education (MEC MAT2005-01388, NAN2004-09109-C04, TEC2004-05260-C02-02, Consolider-CSD 2006-19, and TEC2005-03694) and the Community of Madrid (CAM S-0505-ESP-0200). The authors would also like to thank the SFI/HEA Irish Centre for High-End Computing (ICHEC) for providing computational facilities for the calculations.

[1] M. Weyers, M. Sato, and H. Ando, Jpn. J. Appl. Phys., Part 2 **31**, L853 (1992).
[2] H. Riechert, A. Ramakrishnan, and G. Steinle, Semicond. Sci. Technol. **17**, 892 (2002).
[3] J. F. Geisz and D. J. Friedman, Semicond. Sci. Technol. **17**, 769 (2002).
[4] R. C. Newman, Adv. Phys. **18**, 545 (1969).
[5] M. Stavola, in *Semiconductors and Semimetals*, edited by M. Stavola (Academic, New York, 1999), Vol. 51B, Chap. 4.
[6] M. D. McCluskey, J. Appl. Phys. **87**, 3593 (2000).
[7] T. Prokofyeva, T. Sauncy, M. Seon, M. Holtz, Y. Qiu, S. Nikishin, and H. Temkin, Appl. Phys. Lett. **73**, 1409 (1998).
[8] H. Ch. Alt, A. Yu. Egorov, H. Riechert, B. Wiedemann, J. D. Meyer, R. W. Michelmann, and K. Bethge, Appl. Phys. Lett. **77**, 3331 (2000).
[9] S. Kurtz, J. Webb, L. Gedvilas, D. Friedman, J. Geisz, J. Olson, R. King, D. Joslin, and N. Karam, Appl. Phys. Lett. **78**, 748 (2001).
[10] J. Wagner, T. Geppert, K. Köhler, P. Ganser, and N. Herres, J. Appl. Phys. **90**, 5027 (2001).
[11] T. Geppert, J. Wagner, K. Köhler, P. Ganser, and M. Maier, Appl. Phys. Lett. **80**, 2081 (2002).

[12] A. Mascarenhas and M. J. Seong, Semicond. Sci. Technol. **17**, 823 (2002).
[13] J. Wagner, T. Geppert, K. Köhler, P. Ganser, and M. Maier, Appl. Phys. Lett. **83**, 2799 (2003).
[14] H. Ch. Alt and Y. V. Gomeniuk, Phys. Rev. B **70**, 161314(R) (2004).
[15] M. Güngerich, P. J. Klar, W. Heimbrodt, J. Koch, W. Stolz, M. P. Halsall, and P. Harmer, Phys. Rev. B **71**, 075201 (2005).
[16] E.-M. Pavelescu, J. Wagner, H.-P. Komsa, T. T. Rantala, M. Dumitrescu, and M. Pessa, J. Appl. Phys. **98**, 083524 (2005).
[17] S. Lazić, J. M. Calleja, R. Hey, and K. Ploog, Phys. Status Solidi B **243**, 1634 (2006).
[18] E. Gallardo, S. Lazić, J. M. Calleja, J. Miguel Sánchez, M. Montes, A. Hierro, R. Gargallo-Caballero, A. Guzmán, E. Muñoz, A. M. Teweldeberhan, and S. Fahy, Physica E (to be published).
[19] A. M. Teweldeberhan and S. Fahy, Phys. Rev. B **72**, 195203 (2005).
[20] A. M. Teweldeberhan and S. Fahy, Phys. Rev. B **73**, 245215 (2006).
[21] S. B. Zhang and S.-H. Wei, Phys. Rev. Lett. **86**, 1789 (2001).
[22] R. P. Feynman, Phys. Rev. **56**, 340 (1939).
[23] G. Kresse and J. Hafner, Phys. Rev. B **47**, 558 (1993).
[24] G. Kresse and J. Furthmüller, Phys. Rev. B **54**, 11169 (1996).
[25] J. P. Perdew and A. Zunger, Phys. Rev. B **23**, 5048 (1981).
[26] D. Vanderbilt, Phys. Rev. B **41**, 7892 (1990).
[27] G. Kresse and J. Hafner, J. Phys.: Condens. Matter **6**, 8245 (1994).
[28] H. J. Monkhorst and J. D. Pack, Phys. Rev. B **13**, 5188 (1976).
[29] P. Y. Yu and M. Cardona, *Fundamentals of Semiconductors* (Springer-Verlag, Heidelberg, 1996).
[30] H. M. Cheong, Y. Zhang, A. Mascarenhas, and J. F. Geisz, Phys. Rev. B **61**, 13687 (2000).
[31] A. Y. Liu and A. A. Quong, Phys. Rev. B **53**, R7575 (1996).
[32] G. Stenuit and S. Fahy, Phys. Rev. B (to be published).
[33] T. Mattila, S.-H. Wei, and A. Zunger, Phys. Rev. B **60**, R11245 (1999).
[34] The maximum change in LVM frequency, in going from the 32-atom to the 64-atom supercell, is 9 cm^{-1}.
[35] For GaAs, $E_g^{LDA}=0.55$ eV and $E_g^{exp}=1.52$ eV.